ACS APPLIED ENERGY MATERIALS

www.acsaem.org

Article

Microwave Exfoliated Few-Layered Graphene Cathode for Aluminum Batteries

Published as part of ACS Applied Energy Materials special issue "Global Conference for Decarbonization of Energy and Materials 2023".

Shaikshavali Petnikota,*,⊥ Glaydson Simões Dos Reis,⊥ Fathima Ali Kayakool, Venkata Satya Siva Srikanth Vadali, Juho Välikangas, Ulla Lassi, and Mikael Thyrel

Cite This: ACS Appl. Energy Mater. 2024, 7, 6862−6872

Read Online

ACCESS | Metrics & More | Article Recommendations | Supporting Information

ABSTRACT: Microwave-exfoliated few-layered graphene (meFLG) with oxygen, hydroxyl, and sulfate impurities is tested as a cathode material in aluminum batteries (ABs). The O and S impurities bonded to C atoms are found collectively weighing 2.9−4.7 at. % (4.1−6.9 wt %). meFLG as a cathode in AB pouches delivered stable discharge capacities around 100 mAh/g at 0.1 A/g current rate over 500 cycles, despite high irreversible capacities noticed for the first few cycles. Side reactions of the impurities with the electrolyte species are found to be responsible for the initial high irreversible capacities. The effect of the impurities became negligible when meFLG cycled at higher current rates starting from 1.0 A/g, but initial energy storage capacities and cyclic behavior varied with the voltage window. Postcycling chemical analysis of the electrode matrix revealed that anion species ($AlCl_4^-$) of the electrolyte are found covalently bonded to the impurities, while cation species are found intact even after 500 cycles of continuous charge−discharges. We therefore recommend careful characterization of the impurities before using FLG-related materials as aluminum battery cathode materials. Removing the impurities before the electrode fabrication will help meFLG outperform its class of materials because it shows excellent rate capability even with the impurities.

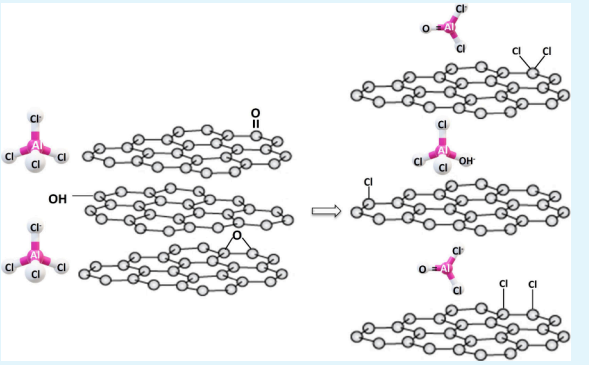

KEYWORDS: *microwave-exfoliation, few-layered graphene, impurities, aluminum batteries, cathode, $AlCl_4^-$ anions*

1. INTRODUCTION

Aluminum battery (AB) technology is touted as a potential alternative to Li-ion battery (LIB) technology due to its several advantages.[1−4] Aluminum is the third most abundant element in the Earth's crust, making it readily available and relatively inexpensive compared to Li. This abundance makes the AB technology a more sustainable and cost-effective option. Aluminum offers a gravimetric energy storage capacity of 2.98 Ah/g, which is comparable to the gravimetric capacity (3.86 Ah/g) of Li, and a higher volumetric capacity of 8.05 Ah/cm^3 compared to the volumetric capacity (2.06 Ah/cm^3) of Li.[1−4] Due to the low reactivity of Al (compared to the hyperactivity of Li) and the high thermal stability (>300 °C) of $AlCl_3$−ionic liquid (IL) electrolytes (compared to low-temperature (<60 °C) tolerance of Li−organic carbonate solvents), AB technology offers safety as a built-in feature. However, a major bottleneck in AB technology is the availability of an efficient and economically viable cathode material, which improves the storage capacity and durability of the AB. Various graphitic carbonaceous materials are being tested as AB cathode materials in this context. However, these materials (such as graphite) either offer low capacities or are expensive to prepare (like in the case of CVD graphene).[1,2,5] Of late, few-layered graphene (FLG) is being tested as an efficient AB cathode material as an alternate to the inefficient and expensive materials.[1,2,6−8] FLG is typically prepared by reducing and exfoliating graphene oxide (GO), commonly prepared by wet-chemical methods that involve oxidizers such as $KMnO_4$ and H_2SO_4. Therefore, FLG is bound to have oxygen and sulfate impurities; those in limited amounts are beneficial for solid electrolyte interface (SEI) formation that further prevents electrolyte decomposition as well as eases ionic movement when it used as LIB anode. Consequently, the electrochemistry of ABs comprised of IL electrolytes is not favorable for SEI formation and it is intriguing to study the

Received: February 27, 2024
Revised: July 15, 2024
Accepted: July 31, 2024
Published: August 14, 2024

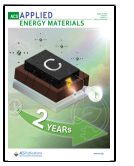

https://doi.org/10.1021/acsaem.4c00444
ACS Appl. Energy Mater. 2024, 7, 6862−6872

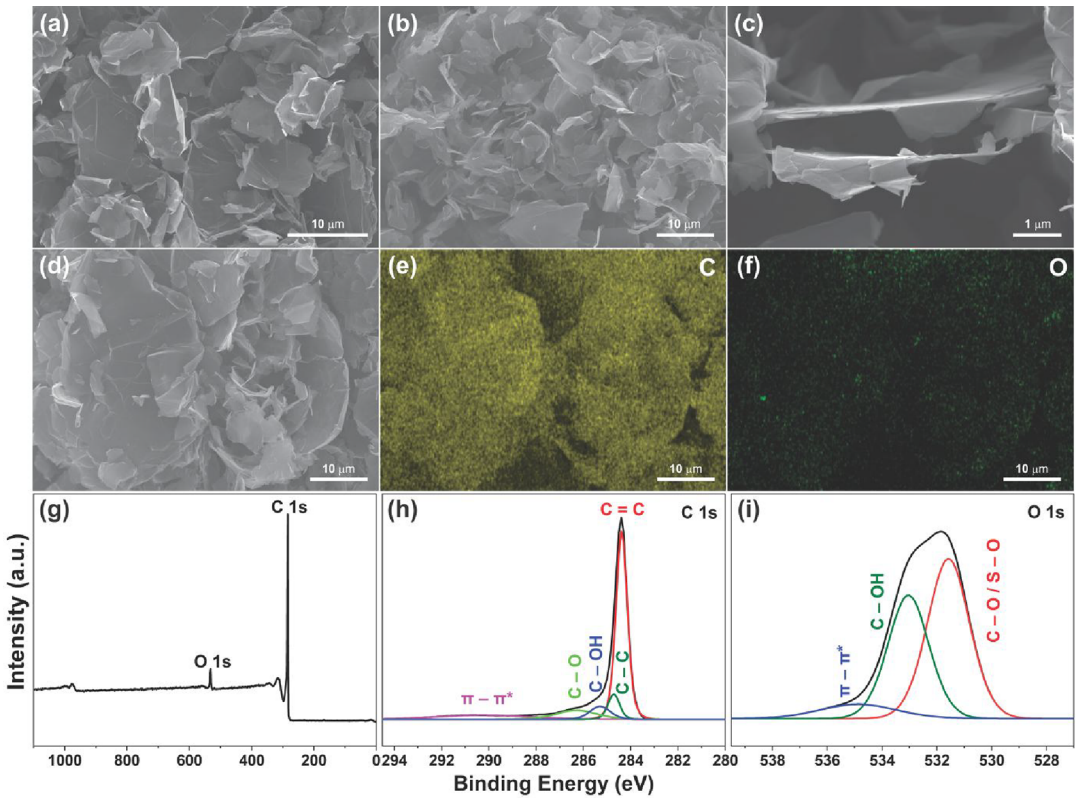

Figure 1. (a–d) Morphology of meFLG under FESEM and corresponding (e) C and (f) O elemental mappings; (g) XPS survey and corresponding high-resolution (h) C 1s and (i) O 1s spectra of meFLG.

influence of the impurities in meFLG on its performance as an AB cathode material. Previously, we prepared FLG by exfoliating GO using a household microwave oven.[9−11] This microwave-exfoliated FLG (meFLG) possessed an excellent extent of exfoliation, a high degree of 2D crystallinity, fewer defects, etc. We demonstrated meFLG as an excellent LIB anode and supercapacitor electrode material.[9−11] Therefore, the hypothesis is that meFLG could perform as an excellent AB cathode material due to its good structural stability and durability during repeated charge and discharge cycles.[1,2,6−8] It could withstand the intercalation and deintercalation of complex tetrachloroaluminate anions ($AlCl_4^-$) without significant structural damage or capacity degradation, leading to improved cycling stability and a longer lifespan for the battery.[2] However, meFLG may possess O, S, OH, etc., impurities (similar to thermally reduced FLG[12]), unlike commercially available wet-jet milling-produced graphene (GWJM; C, ~99.99 at. %)).[2] These impurities may form irreversible covalent compounds (namely, Al_2O_3, $Al(OH)_3$, etc.) by reacting with highly corrosive "$AlCl_3$−1-ethyl-3-methylimidazolium chloride ([EMIM]Cl)" IL, the most commonly used AB electrolyte.[2,3,6,8,13] The formation of these covalent compounds is detrimental to the continuous and safe operation of AB. Therefore, we systematically studied (using chemical and electrochemical analyses) the effect of impurities in meFLG on the performance of the AB pouches when meFLG is used as a cathode material, and the same is reported here.

2. EXPERIMENTAL DETAILS

meFLG prepared in our previous work was considered for this work.[10] Electron microscopy and preliminary elemental analysis (EDX) were carried out with an electron beam at an accelerating voltage of 7 kV using the Zeiss Merlin field emission scanning electron microscope (FESEM). High-precision elemental analysis was carried out using X-ray photoelectron spectroscopy (XPS), which was performed using the Kratos Axis Ultra spectrometer with Al Kα monochromated source operated at 150 W, with a pass energy of 160 and 20 eV for acquiring survey and element-specific spectra. An electrode slurry of meFLG (95 wt %) and NaCMC binder (5 wt %) was prepared using water/ethanol (1:1 by volume) solvent. Then, electrodes of meFLG were fabricated by drop-casting the slurry onto custom-made Mo (thickness 0.1 mm, ≥99.9%, Sigma-Aldrich) substrates and the coatings were dried at 105 °C overnight. Similarly the control graphite (~300 μm) electrodes prepared with 10 wt % PVDF binder using NMP solvent as it does not disperse in water/ethanol. The active mass loading was in the range of 2.5−6 mg uniformly spread over a 2.1 cm^2 rectangular area. AB pouches with the fabricated meFLG and graphite electrodes as cathode, high-purity Al-foil as anode (thickness, 0.25 mm; 99.999%; Sigma-Aldrich), 1.3 M $AlCl_3$:[EMIM]Cl IL as electrolyte, and Whatman GF/D glass microfiber filters as separator are assembled inside an Ar-filled glovebox (MBraun LABstar).[2,3] More details about the electrolyte preparation and pouch cell assembly were reported in our recent publication.[2,3] The cyclic voltammetry and charge−discharge measurements were conducted at room temperature (~25 °C) with the Arbin LBT21084UC system and Maccor Series 4000 battery tester, respectively. CV profiles at multiple scan rates ranging from 0.1 to 1.0 mV/s were measured with a BioLogic SP-150e potentiostat. Electrochemical impedance spectroscopy (EIS) measurements were carried out with an AC signal amplitude of 10 mV in the frequency range of 200000 to 0.1 Hz using BioLogic SP-150e. Raman scattering spectra were obtained with 514.5 nm Ar-ion laser using Renishaw InVia Raman microscope. X-ray diffraction (XRD) patterns were recorded with Cu Kα (λ = 0.154 nm) radiation using PANalytical X'pert[3] powder instrument. The EIS and postcycling Raman and XRD measurements were carried at the room temperature.

https://doi.org/10.1021/acsaem.4c00444
ACS Appl. Energy Mater. 2024, 7, 6862−6872

Table 1. Elemental Analysis of FLG from EDX

	Figure 1d		Figure S1					
			Area 1		Area 2		Area 3	
Element	wt %	at. %	wt %	at. %	wt %	at. %	wt %	at. %
C	95.9	97.09	95.2	97.1	93.0	95.3	94.6	96.5
O	3.55	2.7	3.5	2.7	5.8	4.5	4.3	3.3
S	0.55	0.21	1.3	0.2	1.2	0.2	1.1	0.2

3. RESULTS AND DISCUSSION

The morphology of meFLG with crumpled and fluffy features of the randomly shaped individual meFLG particles with lateral sizes of several micrometers is shown in Figure 1a−d. Individual meFLG particles have very smooth surfaces. Together, they form a 3D structure rich in voids and spaces between the particles, which are expected to enhance contact with the electrolyte, provide effective electron conduction channels, and shorten the ionic diffusion distance, consequently expected to yield high storage capacities. The spaces between the meFLG particles such as those seen in Figure 1c may also accommodate/buffer the possible volume expansion of the electrode matrix during to and fro diffusion of large charge carriers, here $AlCl_4^-$ (~6 Å) anions during charge−discharge cycles of the AB.[3] The elemental composition of meFLG is given in Table 1. Figure 1e,f, and Figure S1a of the Supporting Information (SI) show the corresponding C, O, and S elemental mappings. Areas 1−3 mentioned in Table 1 are shown in Figure S1b. It can be seen that meFLG is composed of C content in the range of 95.3−97.1 at. %. It is also clear that meFLG contains impurities of O and S as high as 4.5 and 0.21 at. %, respectively, as seen in Table 1. The same is inferred from the XPS data given in Table 2. The survey spectrum (Figure 1g) confirms that meFLG mainly consists of C and O elements. The majority of C atoms in meFLG are found in the sp^2 (61.43 at. %) and sp^3 (8.45 at. %) configurations (Figure 1h). The O and OH impurities that are bonded to C atoms are present in significant amounts, as seen in Table 2. The C−O bonds plausibly stem out either from C═O or C−O−C or O−C═O bonding modes.[14] A trace amount (0.18 at. %) of sulfur impurity as sulfate group is also found (Figure 1i), which is in close agreement with the elemental mapping (Figure S1a) as mentioned in Table 1. Overall, the EDX and XPS analyses' inferences strongly agree with each other. The high C content of meFLG is comparable to commercial graphene such as GWJM (C~99.99 at. %),[2] but with significantly high O and S impurities.

Table 2. XPS-Based Chemical Analysis of meFLG

Name	Bonding Mode	Position (eV)	FWHM[a] (eV)	Atomic %
C 1s	C═C	284.38	0.56	61.43
	C−C	284.71	0.57	8.45
	C−OH	285.29	1.02	7.75
	C−O	286.29	2.06	10.80
	$\pi-\pi^*$	290.23	4.61	11.56
O 1s	C−O/S−O	531.60	1.80	1.80
	C−OH	533.00	1.75	1.35
	$\pi-\pi^*$	534.90	4.32	0.29
S $2p_{3/2}$	SO_4^{2-}	168.30	1.40	0.18

[a]FWHM, full width at half-maximum.

The cyclic voltammetry (CV) responses of meFLG and graphite electrodes at 0.1 mV/s scan rate are shown in Figure 2a,b, respectively. meFLG showed three small (a1, a2, and a3) and one large (a4) current peak at 1.93, 2.1, 2.23, and 2.43 V, respectively, during all anodic scans. Subsequent cathodic scans also displayed one large (c1) and three small (c2, c3, and c4) current peaks at 2.2, 2.05, 1.87, and 1.79 V, respectively. On the other hand graphite took a while, say fourth cycle, to expose all of its peaks; that is, a plausibly large lateral size of the graphite flakes (~300 μm) needs additional time for the complete percolation of electrolyte species, which is also known as electrode formation. In total, unlike meFLG, graphite showed six sets of distinct redox peaks, as seen in Figure 2b. These anodic and cathodic peaks are attributed to the insertion and deinsertion of $AlCl_4^-$ anions into the interlayer gaps of meFLG and graphite as described in eqs 1 and 2, respectively. The observed multiple current peaks correspond to various staging events of $AlCl_4^-$ anions.[2,6−8] Equation 3 gives the overall charge storage mechanism. The broad and feeble (a1−a3 and c2−c4) peaks of meFLG appeared steep and strong in the case of graphite, in addition to two sets of extra peaks (Figure 2b). Graphite being built-in with regularly ordered stalking of individual graphene/basal planes along the crystallographic *c*-direction is able to display such strong and distinct peaks. In contrast, meFLG, lacking of such a stalking order, shows fewer and feebler peaks than the graphite. Further, graphite exhibited the intercalation peaks between 1.5 and 2.45 V, whereas meFLG showed both the intercalation and electrochemical absorption−desorption features at all voltages. which is a type of pseudocapacitor behavior. The CV characteristics of meFLG and graphite are in strong agreement with various graphenaceous materials reported.[2,6−8] Moreover, the CV profiles of meFLG showed that cathodic/anodic peaks remained almost at the same position after the first cycle, suggesting that the intercalation/deintercalation reactions are not significantly affected. However, a slight current increase is observed throughout the cycling, indicating the early capacity increase that could be attributed to either the structural reorganization of meFLG or its impurities' side reactions with the electrolyte species.

anode:

$$Al + 7AlCl_4^- \leftrightharpoons 4Al_2Cl_7^- + 3e^- \quad (1)$$

cathode:

$$C_n[AlCl_4] + e^- \leftrightharpoons C_n + AlCl_4^- \quad (2)$$

net reaction:

$$Al + 4AlCl_4^- + 3C_n[AlCl_4] \leftrightharpoons 4Al_2Cl_7^- + 3C_n \quad (3)$$

The charge−discharge profiles of meFLG and graphite at a 0.1 A/g current rate are shown in Figure 2c,d, respectively. The graphite electrode showed clear and distinct multiple charging and discharging plateaus corresponding to intercalation and

https://doi.org/10.1021/acsaem.4c00444
ACS Appl. Energy Mater. 2024, 7, 6862−6872

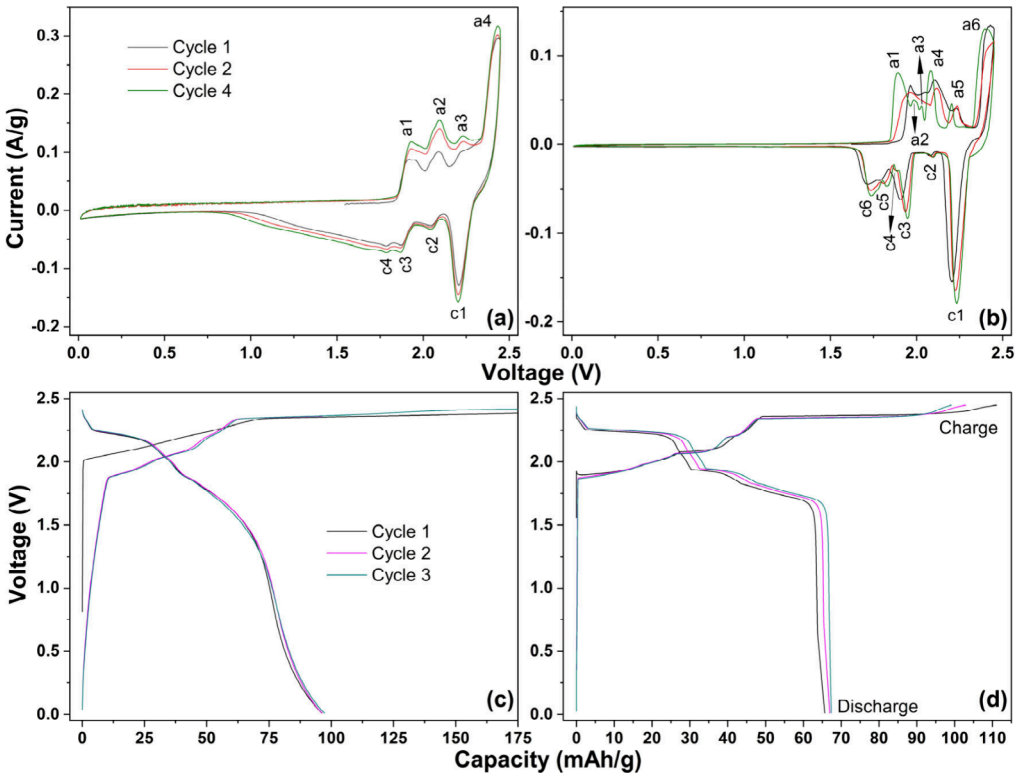

Figure 2. CV profiles of (a) meFLG and (b) graphite at 0.1 mV/s; charge−discharge profiles of (c) meFLG and (d) graphite at 0.1 A/g.

subsequent staging of $AlCl_4^-$ anions between 1.5 and 2.45 V in tune with its CV features. It delivered most of the charge−discharge capacities in this voltage range, as seen in Figure 2d. However, it delivered charge and discharge capacities of 111 mAh/g and 66 mAh/g, respectively, that account for Coulombic efficiency (CE) of 60%. This low CE results in from PVDF's side reaction with the electrolyte and shape readjustments of $AlCl_4^-$ anions.[2,3] Further cycling details of the graphite are beyond the interest of the present work, not pursued for the reason that its large flake size (~300 μm) causes failure at an early stage similar to well-documented commercial graphite (Sigma-Aldrich, ~150 μm).[2] In the case of meFLG, all of the charge curves exhibit sloping plateaus in the range of 1.8−2.4 V, corresponding to the insertion and staging of $AlCl_4^-$ anions into the graphene layers of meFLG particles. The subsequent discharge curves displayed continuous sloping plateaus throughout the voltage window. Both charge−discharge profiles of meFLG are in good agreement with its CV curves. However, the first few charging capacity curves are unusually prolonged to as high as 827 mAh/g, as seen in Figure 2c and Figure S2a. The first discharge capacity is only ~100 mAh/g, leaving an irreversible capacity loss (ICL) of 727 mAh/g. The ICL declined continuously and became negligible from the 100th cycle onward, as seen in Figure 3a. Despite the drastic changes in charge capacities, the discharge capacities remained stable in the 100−150 mAh/g range throughout the cycling (Figure 3a). In general, $AlCl_4^-$ undergoes electrochemical structural distortion from tetrahedral to planar while charging.[5,7] Such a structural change plausibly needs additional energy at low current rates to attain the equilibrium; i.e., charging capacity is more than discharging capacity, thus resulting in low CE.[2,5−8] But, in the present case, the unusually higher charge capacities could be contributed to by the impurities in two possible ways: (1) increased resistance to the intercalation of $AlCl_4^-$ anions and (2) possible side reactions to form irreversible covalent compounds such as Al_2O_3, $Al(OH)_3$, or their intermediaries, etc. Nonetheless, continuous electrolyte decomposition is impossible as it remains stable up to 2.5 V.[3,15] The ICL reduced significantly when the voltage window is lowered to 0.5−2.41 V, but the cycling behavior did not change much, as seen in Figure 3b and Figure S2b. Interestingly, at 1.0 A/g current rate cycling, ICL values became negligible in both voltage windows, as seen in Figure 3c,d. In both voltage windows, initial CEs are greater than 95% and soon attained 100%, as seen in Figure S3a,b. In both cases, initial capacities continuously increased and declined that could be ascribed to electrode formation followed by structural reorganization.[2] However, in the 0.01−2.45 V window (Figure 3c), the capacities stabilized around 45 mAh/g from cycle 1000 onward with identical charge−discharge profiles (Figure S2c). On the other hand, in the 0.5−2.41 V voltage window, the end capacities continuously increased (Figure 3d) and corresponding charge−discharge profiles (Figure S2d) indicated that meFLG underwent continuous structural changes similar to commercial graphene, GWJM.[2] Further increases in the current rate, as seen in rate capability tests, secured 100% CE values throughout the cycling (Figure 3e,f). The different cycling behaviors and the extent of ICL, i.e., the side reactions (Figure 3c,d), confirm that voltage cutoff plays a crucial role. The negligible ICL values at higher current rates indicate that either (1) the side reactions of impurities postponed to higher cycle numbers and/or (2) a major contribution to unusual charge capacities seen during 0.1 A/g cycling is due to the obstruction of $AlCl_4^-$ ions' diffusion by the impurities. It appears that the electrical energy associated with a low current rate is not enough to overcome the obstacles instantaneously, as seen in the case of higher current rates. Another plausible

https://doi.org/10.1021/acsaem.4c00444
ACS Appl. Energy Mater. 2024, 7, 6862−6872

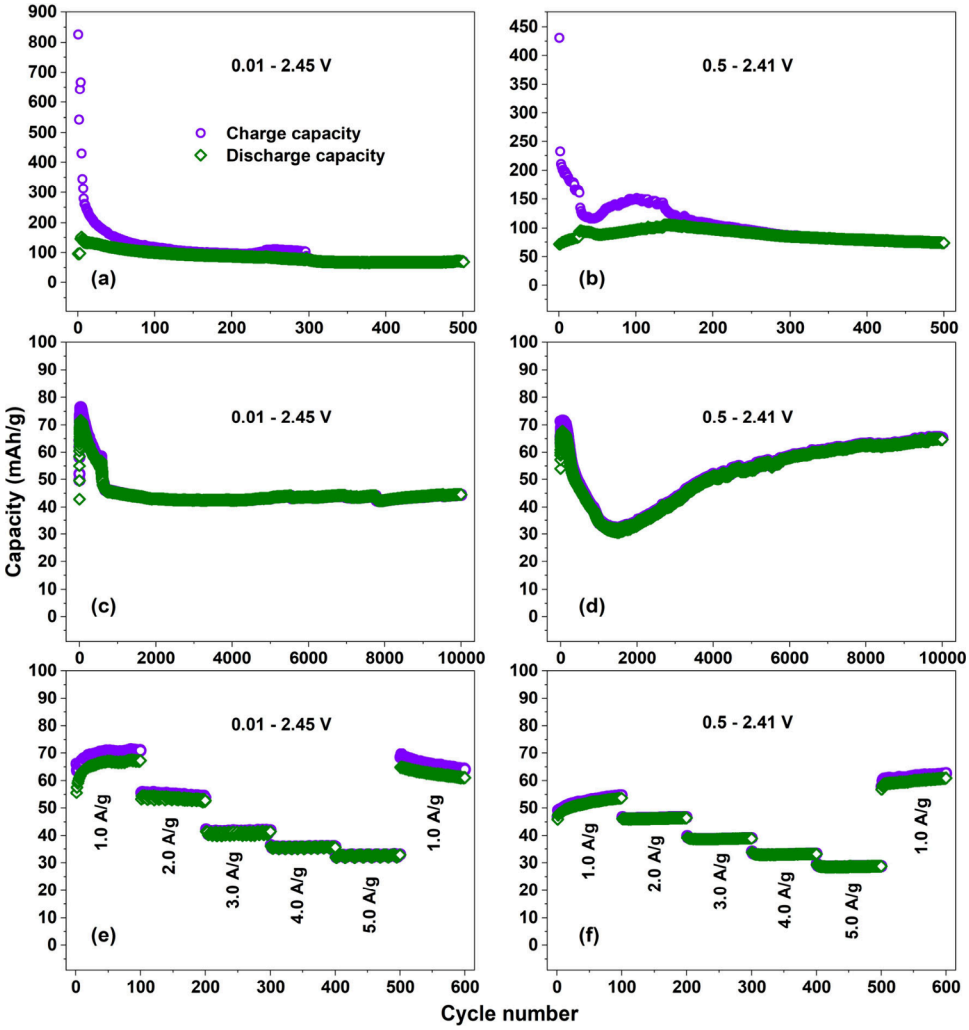

Figure 3. (a, b) Cycling behavior at 0.1 A/g, (c, d) long-term cycling at 1.0 A/g, and (e, f) rate capability of meFLG.

reason behind the low ICL values could be the C-rate effect; i.e., at high current rates, part of the electrode matrix either becomes inactive or the side reactions formation time shortens.[16,17] The inactive part of the electrode material can be reactivated at low C-rates.[16] Further, the normal intercalation of $AlCl_4^-$ anions emerges once the side reactions annihilate the impurities ultimately. Therefore, it is evident that meFLG could perform better by either obliterating the impurities before using it as a cathode material or by simply charging the cathode at higher currents. Nevertheless, the performance of meFLG is similar to the commercial FLG materials such as GWJM, as seen in its rate capabilities (Figure 3e,f and Figure S2e,f), especially in the 0.01−2.45 V window. meFLG delivered discharge capacities of 68, 55, 42, 36, 33, and 68 mAh/g at 1.0, 2.0, 3.0, 4.0, 5.0, and 1.0 A/g current densities, respectively (Figure 3e). The high capacities and good rate capability of meFLG are attributed to the outstanding electronic conductivity and 2D mechanical stabilities of individual graphene layers in it. In addition, the stable and identical charge−discharge curves (Figure S2e,f) indicate that the meFLG cathode possesses a highly stable 2D structure that is resilient to structural changes even with extensive cycling. Nonetheless it will be intriguing to completely remove the impurities from the meFLG and perform a comprehensive comparison between defective meFLG and impurity-free meFLG. This forms the scope of our future work. Further, modifying the properties of meFLG or its electrode similar to biomass derived activated carbons and bioinspired carbon electrodes not only improves the ABs performance but also benefits the design of better metal-ion batteries (MIBs) such as Li-, Na-, K-, Zn-, and Al-ion batteries.[4,18] Also trying bioinspired carbon electrode materials as cathodes in Al-ion batteries is in our future scope of work. These carbon electrodes are touted to exhibit enhanced specific capacitance, cyclic stability, and capacity retention.[4,18] If carefully designed, the Al-ion storage and conductivity can also be enhanced.[19] More importantly, these carbons offer enhanced mechanical robustness, and thereby, they may aid in mitigating the mechanical stress buildup and sudden structure collapse during cycling. Utilizing 3D printing may further improve the performance of these cathode materials in Al-ion batteries and other MIBs.

Interactions of the impurities with both cations ($EMIM^+$) and anions ($AlCl_4^-$) of the electrolyte are evaluated with XPS and corresponding results are shown in Figure 4, Figure S4, and Table 3. The discharged electrode that aged for 500 cycles (Figure 3a) is considered to pinpoint the permanent changes that occurred to both anion and cation species of the electrolyte as well as meFLG. The C 1s spectrum displayed C−(C, H) bonds of meFLG and aliphatic chains of $EMIM^+$

https://doi.org/10.1021/acsaem.4c00444
ACS Appl. Energy Mater. 2024, 7, 6862−6872

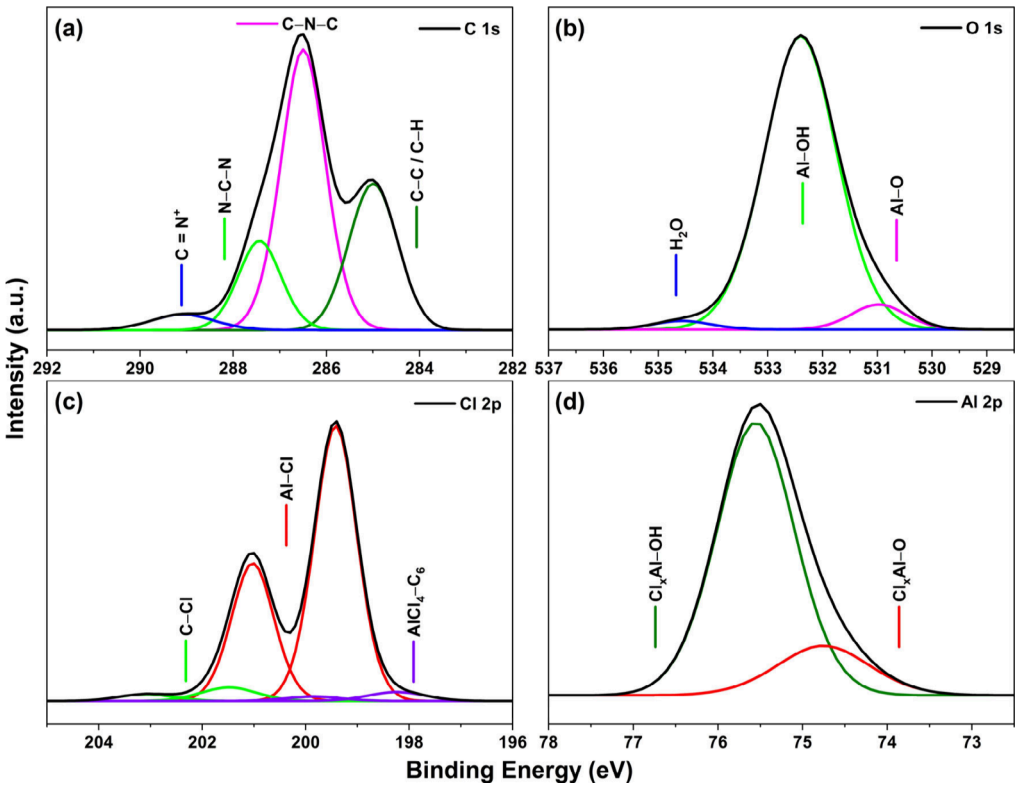

Figure 4. XPS high-resolution (a) C 1s, (b) O 1s, (c) Cl 2p, and (d) Al 2p spectra of cycled meFLG electrode.

Table 3. XPS-Based Chemical Analysis of meFLG

Name	Bonding Mode	Position (eV)	FWHM[a] (eV)	Atomic %
C 1s	C−(C, H)	285.0	1.15	14.94
	C−N−C	286.5	1.1	26.53
	N−C−N	287.4	1.05	8.15
	C═N$^+$	289.1	1.55	2.09
O 1s	Al−O	531.0	1.15	0.36
	Al−OH	532.4	1.55	5.6
	surface OH	533.6	1.25	0.13
N 1s	−N$^-$−	399.8	1.45	0.57
	N−C	401.9	1	11.89
Cl 2p$_{3/2}$	$AlCl_4$−C_6	198.3	1.3	0.9
	Al −Cl	199.4	0.95	20.18
	C−Cl	201.5	1.25	1.32
Al 2p	Al−O	74.8	1.25	1.3
	Al−OH	75.6	1.05	6.03

[a]FWHM, full width at half-maximum.

cation at 285.0 eV, while various C−N bonds of EMIM$^+$ cation were between 285.0 and 291.0 eV as seen in Figure 4a.[20,21] The N 1s spectrum too exhibited C−N bonds of EMIM$^+$ cation (Figure S4). Binding energies of the C−N bonds (Table 3) are in good agreement with the imidazole ring of multiple ionic salts reported and confirm that EMIM$^+$ cation species are intact.[20−24] The peaks at 531.0 and 532.4 eV of O 1s spectrum (Figure 4b) represent O (Al−O/Al═O) and OH bonded to Al, respectively.[25,26] The bonding modes of the O 1s spectrum match Al_2O_3 and $Al(OH)_3$ compounds and confirm their formation. A major proportion of the Cl 2p spectrum corresponds to Al − Cl bonds of $AlCl_4^-$ and a part of it is found interacting with carbon hexagons (C_6) of meFLG (Figure 4c).[23,27] The two peaks of the Al 2p spectrum at 74.8 and 75.6 eV correspond to $AlCl_4^-$ anions altered with O and OH bonds, respectively (Figure 4d).[25,27] Therefore, unlike the cation case, anion species, i.e., $AlCl_4^-$ anions, mainly underwent major changes as if some of their chlorines were covalently replaced by oxygen and hydroxyl moieties. Part of the replaced chlorines were found bonded to carbons of meFLG (Figure 4c).[28] Some of these possible reactions are described in eqs 4−6, carbons of meFLG represented as ">C". Furthermore, these XPS findings point out that the impurities of meFLG certainly swapped by the electrolyte species, particularly by the anions. In general, at higher current densities, charge carriers involved in conversion reactions at a later stage of cycling[29] and the XPS inferences confirm that the side reactions plausibly postponed to higher cycle numbers in the case of high current rates cycling (Figure 3c,d).

$$>C-OH + AlCl_4^- \rightarrow >C-Cl + HO-AlCl_3^-/Cl_3Al-OH^- \quad (4)$$

$$>C=O + AlCl_4^- \rightarrow >C<^{Cl}_{Cl} + O=AlCl_2^- \quad (5)$$

$$>C-O-C< + AlCl_4^- \rightarrow 2>C-Cl + O=AlCl_2^- \quad (6)$$

It is intriguing to quantify the diffusion and capacitive storage of charge carriers that occur at all the voltages, as seen in the meFLG's CV characteristics (Figure 2a). The respective storage contributions are quantified by solving eqs 7 and 8.[9] The current responses $i(v)$ at multiple scan rates and particular voltages, as seen in Figure 5a,c, are plotted against the square root of scan rate (v) (eq 8) as shown in Figure 5b,d for obtaining k_1 and k_2 values.[9] The straight lines observed in Figure 5b,d fit into eq 8, which is a $y = mx + c$ type of linear relation in which the slope (m) and intercept (c) are k_1 and k_2,

https://doi.org/10.1021/acsaem.4c00444
ACS Appl. Energy Mater. 2024, 7, 6862−6872

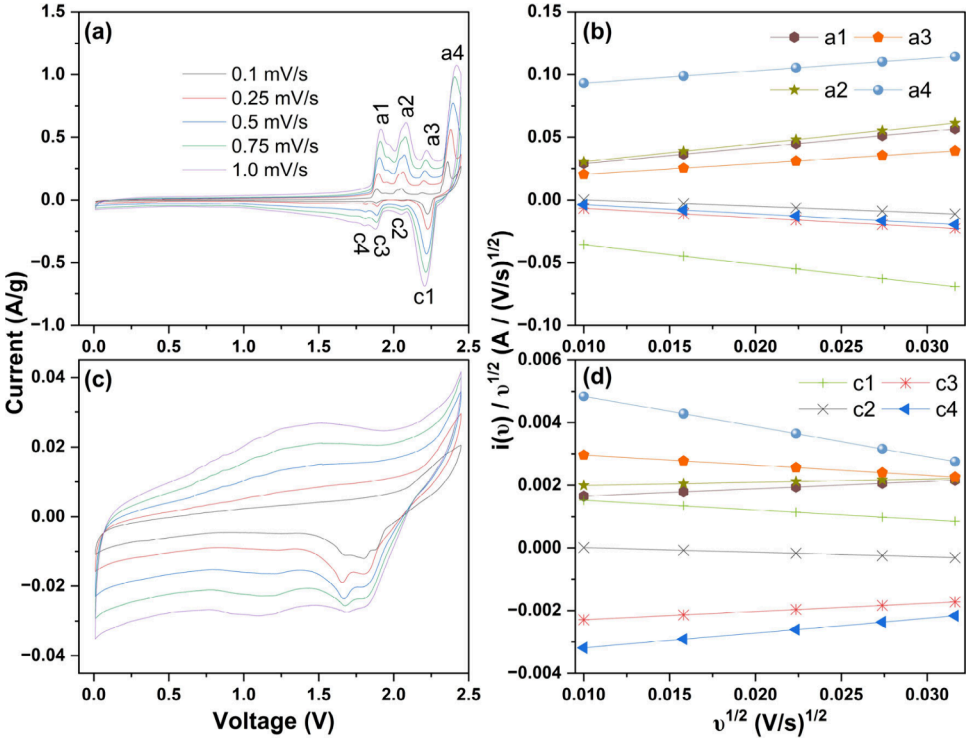

Figure 5. Multiple scan rate CV profiles of meFLG (a) before and (c) after long-term cycling; (b, d) corresponding current ($i(v)$) versus scan rate (v) plots.

Table 4. Diffusion ($k_2v^{1/2}$) and Surface (k_1v) Current Contributions Calculated from Equation 8

	0.1 mV/s				1.0 mV/s			
	Fresh electrode		After 10000 cycles[a]		Fresh electrode		After 10000 cycles[a]	
E (V)	$k_2v^{1/2}$ (%)	k_1v (%)	$k_2v^{1/2}$ (%)	k_1v (%)	$k_2v^{1/2}$ (%)	k_1v (%)	$k_2v^{1/2}$ (%)	k_1v (%)
0.1	85.97	14.03	75.88	24.12	65.96	34.04	49.88	50.12
0.25	55.63	44.37	67.26	32.74	28.39	71.61	39.38	60.62
0.5	47.52	52.48	52.04	47.96	22.26	77.74	25.54	74.46
0.75	25.24	74.76	22.24	77.76	09.65	90.35	8.30	91.70
1.0	5.57	94.43	14.51	85.49	01.83	98.17	5.09	94.91
1.25	11.70	88.30	31.68	68.32	04.02	95.98	12.79	87.21
1.5	17.31	82.69	51.95	48.05	06.21	93.79	25.48	74.52
a1	56.22	43.78	85.94	14.06	28.88	71.12	65.91	34.09
a2	53.88	46.12	94.95	05.05	26.97	73.03	85.62	14.38
a3	57.01	42.99	90.99	09.01	29.55	70.45	76.16	23.84
a4	89.52	10.48	85.74	14.26	72.98	27.02	65.52	34.48
c1	56.82	43.18	85.45	14.55	29.38	70.62	65.00	35.00
c2	50.52	49.48	51.75	48.25	24.41	75.59	25.33	74.67
c3	10.40	89.60	90.67	09.33	03.54	96.46	75.45	24.55
c4	32.64	67.36	88.60	11.40	13.29	86.71	70.99	29.01
1.5	16.06	83.94	90.24	09.76	05.70	94.30	74.51	25.49
1.25	13.75	86.25	65.81	34.19	04.80	95.20	37.84	62.16
1.0	24.95	75.05	57.64	42.36	09.51	90.49	30.08	69.92
0.75	16.65	83.35	65.38	34.62	05.94	94.06	37.39	62.61
0.5	25.65	74.35	78.89	21.11	00.17	99.83	54.17	45.83
0.25	34.65	65.35	80.71	19.29	14.36	85.64	56.95	43.05
0.1	53.25	46.75	88.32	11.68	26.48	73.52	70.51	29.49

[a]Voltages for a1−a4 and c1−c4 peaks considered the same as in the fresh electrode.

respectively. The values of k_1v and $k_2v^{1/2}$ represent the surface and diffusion contributions, respectively. The percentages of surface and diffusion contributions are obtained before and after long-term cycling of about 10000 cycles at 1.0 A/g (after Figure 3c) to shed light on the changes in the storage mechanism with the cycling. The charge carrier's storage mechanism is expected to change dramatically over cycling as meFLG is prone to undergo in situ electrochemical

https://doi.org/10.1021/acsaem.4c00444
ACS Appl. Energy Mater. 2024, 7, 6862−6872

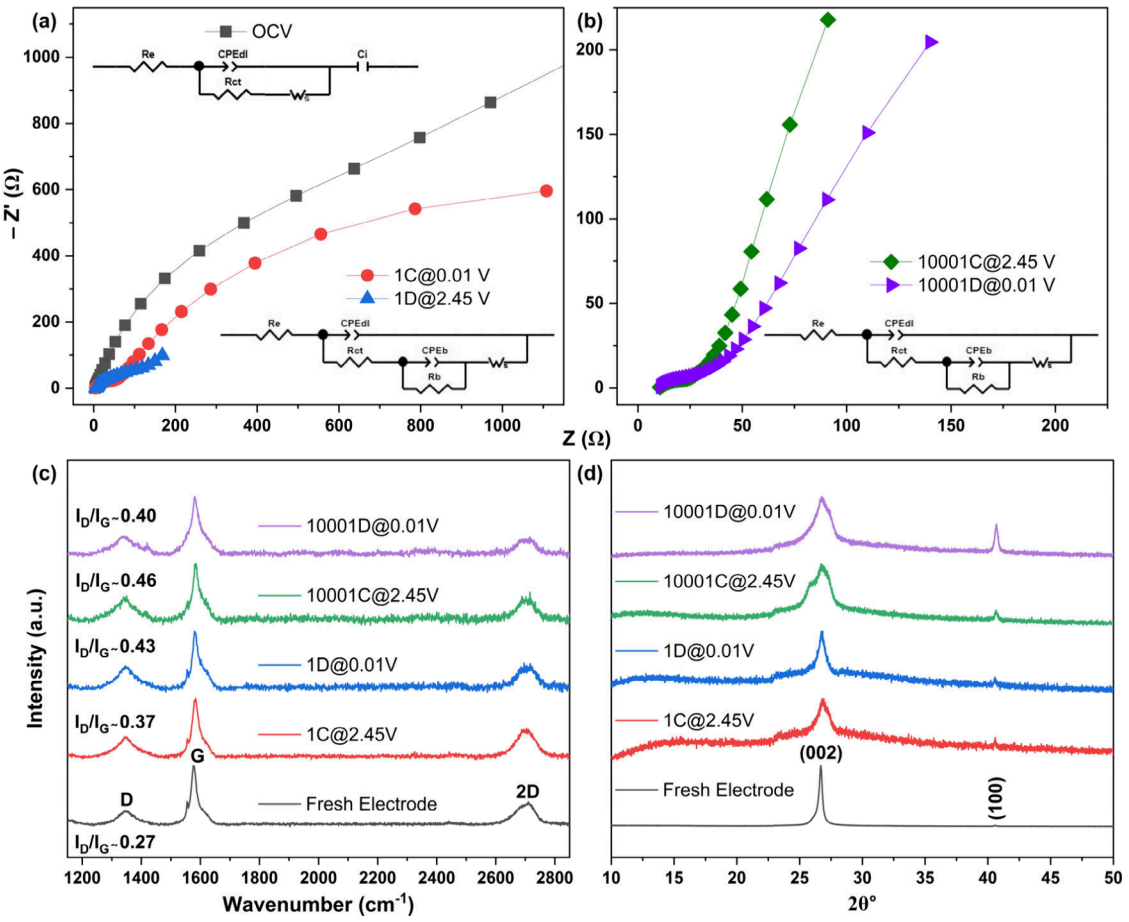

Figure 6. (a, b) Nyquist plots and ECs, (c) Raman spectra, and (d) XRD patterns of meFLG at various charge−discharge conditions before and after long-term cycling.

exfoliation.[2,9,30,31] These changes in the capacitive and diffusion contributions are enumerated in Table 4, which shows that, at 0.1 mV/s scan rate, fresh meFLG electrode exhibited increasing surface current domination up to 1.5 V, and then the trend shifted to diffusion domination for all anodic peaks a1 (1.89 V), a2 (2.05 V), a3 (2.19), and a4 (2.36) and subsequent cathodic peaks c1 (2.23 V) and c2 (2.05 V). The trend again became surface-dominated at c3 (1.88 V), c4 (1.81), and all remaining cathodic voltages. However, surface currents dominated overwhelmingly when the scan rate sequentially increased from a rate of 0.25 to 1.0 mV/s. The charge carriers are predominantly surface adsorbing and desorbing only. In general, low scan rates are associated with diffusion-controlled ionic transport, whereas higher scan rates favor the surface-transport phenomena.[32] Therefore, at higher scan rates, $AlCl_4^-$ anions adsorb/desorb onto meFLG's surfaces very quickly rather than diffusing slowly through it. This inference is in good agreement with the charge−discharge cycles at higher current densities, in which the side reactions of impurities are not observed clearly. The fast adsorption/desorption of $AlCl_4^-$ anions seems to suggest that they do not have enough time to interact with the impurities. Further, it is worth noting that, at 0.1 V of both anodic and cathodic scans, diffusion currents suddenly increased contrary to the subsequent trends. This abnormal change could plausibly be related to the change in the polarity of the applied voltage that prompts the reversal of the ionic flow direction in a diffusing manner. CV profiles of meFLG (Figure 5c) after 10000 continuous charges−discharges at 1.0 A/g current density are in tune with the commercial FLG.[2] All of the anodic and cathodic peaks appear merged into one broad hump-like peak whose current reduction seems compensated for by increased area between 0.01 and 1.5 V. The observed change in CV profiles can be ascribed to permanent structural changes in meFLG. In general, FLG particles undergo in situ electrochemical exfoliation up to 3−5 layers, and further permanent exfoliation or collapse is not possible.[2,30] Absence of current peaks in cycled meFLG (Figure 5c) confirms its full-scale exfoliation. Because of this reason diffusion currents emerged as major contributors at all voltages in 0.1 mV/s scans and between the 1.5 and 2.45 V range in the case of the 1.0 mV/s scan. Here, $AlCl_4^-$ anions seem to diffuse in and out of 3−5 individual graphene layers only, as neither the structural changes nor the side reactions take place. Overall, pre- and postcycling CV curves are in good agreement with the galvanostatic cycling and the postcycling XPS analysis.

$$i(v) = k_1 v + k_2 v^{1/2} \tag{7}$$

$$i(v)v^{-1/2} = k_1 v^{-1/2} + k_2 \tag{8}$$

The charge storage kinetics of meFLG electrodes at different charge−discharge states are probed with EIS. The EIS data plotted as Nyquist plots and fitted to equivalent circuits (ECs) are shown in Figure 6a,b.[9,29,31,33] The values of each circuit element in ECs are given in Table 5. Fresh meFLG electrode displayed higher resistance to charge transfer (R_{ct}) and the

https://doi.org/10.1021/acsaem.4c00444
ACS Appl. Energy Mater. 2024, 7, 6862−6872

Table 5. EIS Data of meFLG in Various Charge−Discharge Conditions of Fresh and Post Long-Term Cycling

	R_e (Ω)	R_{ct} (Ω)	R_b (Ω)	W_s (Ω)
OCV	3.75	1086		3720
1C at 2.45 V	4.94	51.8	10.36	570.1
1D at 0.01 V	4.24	1.41	299.1	253.1
10001C at 2.45 V	10.5	14.0	1053	877.2
10001D at 0.01 V	10.6	17.3	405.8	739.8

diffusion of charge carriers (W_s) at the open circuit voltage (OCV), suggesting the inertness of the electrode matrix to the spontaneous reactions with the electrolyte. After the first charge to 2.45 V (1C), the corresponding EC became complex with greatly decreased R_{ct} and W_s values and considerable contribution from the bulk resistance (R_b, due to substrate, binder, connecting tabs, etc.).[33] as shown in Table 5. After the first discharge to 0.01 V (1D), R_{ct} decreased by 37 times while R_b increased by 29 times, indicating that most of the changes happened during the first charge. After the long-term cycling, a 10-fold increase in R_{ct} was noticed while the contact resistance (R_e) doubled, plausibly owing to the saturated structural and chemical changes. It is worth noticing that after 1D, R_b was found to be several hundred times greater than R_{ct}, indicating fast faradaic charge transfer, and the conductor-like behavior of the electrode matrix.[33]

To access the chemical and structural changes, ex situ Raman spectra (Figure 6c) and XRD patterns (Figure 6d) of five different meFLG electrodes at different stages of charge−discharge states are recorded and analyzed. In all Raman spectra (Figure 6c), the typical D, G, and 2D bands centered at around 1345, 1580, and 2700 cm^{-1}, respectively, are recorded. It is clear from the Raman spectra that there is a negligible change in the band positions in all cases, implying integrity of the electrodes with respect to the chemical bondings at different charge−discharge states. Here, G band stems from pristine and ordered sp^2 carbon hexagons vibrating in E_{2g} mode, whereas D and 2D bands arise from the structural flaws in the basal planes or individual graphene layers such as carbon deficiencies, carbons bonded to the impurities, etc.[2,9,10] The intensity ratio I_D/I_G, which is a direct measure of the extent of defects/disorder, increased by ∼1.4 times after 1C. However, in the case of remaining charge−discharge states, it increased only slightly, as shown in Figure 6c. It is intriguing to notice that the disorder after the 1C is found within the same range throughout the cycling, suggesting that most of the chemical changes occurred during the first charge. The observed increase in the disorder is plausibly due to the detachment of impurities to create more sp^3 carbons (among which some of them bonded to chlorine). On the other hand, the intensity of the 2D band slightly increased and acquired more symmetry after the 1C, indicating uniform expansion of *d*-spacing due to the insertion of $AlCl_4^-$ anions. The shoulder-like feature observed for the fresh electrode could be deconvoluted into $2D_1$ and $2D_2$, corresponding to FLG and graphitic phases, respectively.[2] This shoulder-like feature was not prominent as the charge carrier's insertion took place with cycling.[2] The flattening of this shoulder-like feature is a consequences of the stalking order collapse along the crystallographic *c*-direction.[2,9,10,14] Interestingly, the G band was found to be intact throughout the cycling, providing solid evidence for exceptional chemical inertness and robustness of the 2D-structural integrity of individual graphene layers of meFLG as perceived by the stable charge storage mechanism through its identical charge−discharge curves. All of the Raman scattering observations are in close agreement with the other reported FLGs.[2,9,10]

The XRD pattern of fresh meFLG electrode shown in Figure 6d depicts the characteristic graphitic (002) diffraction peak as the prominent one along with a feeble (100) diffraction peak. The (002) peak broadened to a great extent after the 1C, indicating uniform expansion of *d*-spacing due to the insertion of $AlCl_4^-$ anions,[2] also observed in the case of Raman scattering analysis. In other words, this observation also indicates distortion in the stalking order along the crystallographic *c*-direction. This stalking disorder appears to be irreversible as evidenced by the similarity between XRD patterns corresponding to 1D and 1C. This confirms that most of the structural changes occurred during the 1C and that the disorder increase inferred from the I_D/I_G ratio is mainly due to the prolonged side reactions of the impurities as observed from the unusual charge capacities. The XRD patterns corresponding to charge−discharge states at the end of the long-term cycling appeared similar, except for the reflections from (100) planes, which appeared intense. It is worth noticing that (100) planes are perpendicular to (002) planes, and their strong evolution indicates that part of the exfoliating basal planes or individual graphene sheets are aligned vertically. Such a reorientation was also confirmed in the case of commercial FLG, both experimentally and theoretically, recently.[2] Therefore, postcycling EIS, Raman scattering, and XRD studies of meFLG are self-consistent and corroborative.

4. CONCLUSIONS

In summary, we demonstrated meFLG as an AB cathode material. The oxygen and other impurities associated with meFLG adversely affected the low current rate cycling. However, the AB pouches delivered stable discharge capacities of approximately 100 mAh/g. The effect of impurities was found to be negligible at higher current rates. As a cathode of AB pouches, meFLG exhibited excellent structural stability and durability during continuous charge−discharges over 10000 cycles. It delivered excellent rate capabilities of 68, 55, 42, 36, 33, and 68 mAh/g at 1.0, 2.0, 3.0, 4.0, 5.0, and 1.0 A/g current densities, respectively, with CE values in the range of 95−100%, which is comparable to commercial FLG. Postcycling XPS analysis confirmed that the impurities predominantly interacted with anion species of the electrolyte. The outcomes of the present study suggest that meFLG could perform far better if the impurities are removed before using it as a cathode material, and we recommend further full-scale study in this direction.

■ ASSOCIATED CONTENT

Supporting Information

The Supporting Information is available free of charge at https://pubs.acs.org/doi/10.1021/acsaem.4c00444.

Elemental mapping of S, selected areas 1−3 considered for EDX, voltage versus capacity curves, CEs during the long-term cycling, and N 1s high-resolution spectrum of meFLG (PDF)

https://doi.org/10.1021/acsaem.4c00444
ACS Appl. Energy Mater. 2024, 7, 6862−6872

AUTHOR INFORMATION

Corresponding Author

Shaikshavali Petnikota − *Biomass Technology Centre, Department of Forest Biomaterials and Technology, Swedish University of Agricultural Sciences, SE-90183 Umeå, Sweden;* orcid.org/0000-0001-9269-7447; Email: shaikshavali.petnikota@slu.se, psvali85@gmail.com

Authors

Glaydson Simões Dos Reis − *Biomass Technology Centre, Department of Forest Biomaterials and Technology, Swedish University of Agricultural Sciences, SE-90183 Umeå, Sweden;* orcid.org/0000-0001-8727-9793

Fathima Ali Kayakool − *School of Engineering Sciences and Technology, University of Hyderabad, Hyderabad 500046 Telangana, India*

Venkata Satya Siva Srikanth Vadali − *School of Engineering Sciences and Technology, University of Hyderabad, Hyderabad 500046 Telangana, India;* orcid.org/0000-0002-3021-0987

Juho Välikangas − *Research Unit of Sustainable Chemistry, University of Oulu, FI-90014 Oulu, Finland; Unit of Applied Chemistry, University of Jyvaskyla, Kokkola University Consortium Chydenius, FI-67100 Kokkola, Finland*

Ulla Lassi − *Research Unit of Sustainable Chemistry, University of Oulu, FI-90014 Oulu, Finland; Unit of Applied Chemistry, University of Jyvaskyla, Kokkola University Consortium Chydenius, FI-67100 Kokkola, Finland;* orcid.org/0000-0001-5319-9525

Mikael Thyrel − *Biomass Technology Centre, Department of Forest Biomaterials and Technology, Swedish University of Agricultural Sciences, SE-90183 Umeå, Sweden*

Complete contact information is available at: https://pubs.acs.org/10.1021/acsaem.4c00444

Author Contributions

⊥S.P. and G.S.D.R. contributed equally to this work.

Notes

The authors declare no competing financial interest.

ACKNOWLEDGMENTS

This research was funded by Bio4Energy—a Strategic Research Environment appointed by the Swedish government and the Swedish University of Agricultural Sciences. F.A.K. thanks the Prime Minister's Research Fellows scheme for providing fellowship and support to travel to Sweden.

REFERENCES

(1) Lin, M.-C.; Gong, M.; Lu, B.; Wu, Y.; Wang, D.-Y.; Guan, M.; Angell, M.; Chen, C.; Yang, J.; Hwang, B.-J.; et al. An ultrafast rechargeable aluminium-ion battery. *Nature* **2015**, *520* (7547), 324−328.

(2) Petnikota, S.; Koch, D.; Imran, M.; Buha, J.; Panda, J. K.; Akbari Garakani, M.; Marasco, L.; Gamucci, A.; Bonaccorso, F.; Pellegrini, V. Spray-coated few-layer graphene as an aluminium battery cathode. *Sustainable Energy & Fuels* **2022**, *6* (18), 4311−4321.

(3) Petnikota, S.; Chua, R.; Boopathi, K. M.; Satish, R.; Bonaccorso, F.; Pellegrini, V.; Srinivasan, M. An Insight into the Electrochemical Activity of Al-doped V_2O_3. *J. Electrochem. Soc.* **2020**, *167* (10), 100514.

(4) Reis, G. S.; Petnikota, S.; Subramaniyam, C. M.; de Oliveira, H. P.; Larsson, S.; Thyrel, M.; Lassi, U.; García Alvarado, F. Sustainable Biomass-Derived Carbon Electrodes for Potassium and Aluminum Batteries: Conceptualizing the Key Parameters for Improved Performance. *Nanomaterials* **2023**, *13* (4), 765.

(5) Wang, D.-Y.; Wei, C.-Y.; Lin, M.-C.; Pan, C.-J.; Chou, H.-L.; Chen, H.-A.; Gong, M.; Wu, Y.; Yuan, C.; Angell, M.; et al. Advanced rechargeable aluminium ion battery with a high-quality natural graphite cathode. *Nat. Commun.* **2017**, *8* (1), 14283.

(6) Uemura, Y.; Chen, C.-Y.; Hashimoto, Y.; Tsuda, T.; Matsumoto, H.; Kuwabata, S. Graphene Nanoplatelet Composite Cathode for a Chloroaluminate Ionic Liquid-Based Aluminum Secondary Battery. *ACS Appl. Energy Mater.* **2018**, *1* (5), 2269−2274.

(7) Childress, A. S.; Parajuli, P.; Zhu, J.; Podila, R.; Rao, A. M. A Raman spectroscopic study of graphene cathodes in high-performance aluminum ion batteries. *Nano Energy* **2017**, *39*, 69−76.

(8) Das, S.; Graphene, K. A Cathode Material of Choice for Aluminum-Ion Batteries. *Angew. Chem., Int. Ed.* **2018**, *57* (51), 16606−16617.

(9) Maseed, H.; Petnikota, S.; Srikanth, V. V. S. S.; Rotte, N. K.; Srinivasan, M.; Bonaccorso, F.; Pellegrini, V.; Reddy, M. V. A new insight into Li-staging, in-situ electrochemical exfoliation, and superior Li storage characteristics of highly crystalline few-layered graphene. *J. Energy Storage* **2021**, *41*, No. 102908.

(10) Petnikota, S.; Rotte, N. K.; Srikanth, V. V. S. S.; Kota, B. S. R.; Reddy, M. V.; Loh, K. P.; Chowdari, B. V. R. Electrochemical studies of few-layered graphene as an anode material for Li ion batteries. *J. Solid State Electrochem.* **2014**, *18* (4), 941−949.

(11) Rotte, N. K.; Naresh, V.; Muduli, S.; Reddy, V.; Srikanth, V. V. S.; Martha, S. K. Microwave aided scalable synthesis of sulfur, nitrogen co-doped few-layered graphene material for high-performance supercapacitors. *Electrochim. Acta* **2020**, *363*, No. 137209.

(12) Müllner, S.; Held, T.; Tichter, T.; Rank, P.; Leykam, D.; Jiang, W.; Lunkenbein, T.; Gerdes, T.; Roth, C. Impact of Functional Groups in Reduced Graphene Oxide Matrices for High Energy Anodes in Lithium-Ion Batteries. *J. Electrochem. Soc.* **2023**, *170* (7), No. 070523.

(13) Reed, L. D.; Menke, E. The Roles of V2O5 and Stainless Steel in Rechargeable Al−Ion Batteries. *J. Electrochem. Soc.* **2013**, *160* (6), A915−A917.

(14) Petnikota, S.; Maseed, H.; Srikanth, V. V. S. S.; Reddy, M. V.; Adams, S.; Srinivasan, M.; Chowdari, B. V. R. Experimental Elucidation of a Graphenothermal Reduction Mechanism of Fe_2O_3: An Enhanced Anodic Behavior of an Exfoliated Reduced Graphene Oxide/Fe_3O_4 Composite in Li-Ion Batteries. *J. Phys. Chem. C* **2017**, *121* (7), 3778−3789.

(15) Schoetz, T.; Ueda, M.; Bund, A.; Ponce de Leon, C. Preparation and characterization of a rechargeable battery based on poly-(3,4-ethylenedioxythiophene) and aluminum in ionic liquids. *J. Solid State Electrochem.* **2017**, *21* (11), 3237−3246.

(16) Li, J.; Hwang, S.; Guo, F.; Li, S.; Chen, Z.; Kou, R.; Sun, K.; Sun, C.-J.; Gan, H.; Yu, A.; et al. Phase evolution of conversion-type electrode for lithium ion batteries. *Nat. Commun.* **2019**, *10* (1), 2224.

(17) Leißing, M.; Horsthemke, F.; Wiemers-Meyer, S.; Winter, M.; Niehoff, P.; Nowak, S. The Impact of the C-Rate on Gassing During Formation of NMC622 II Graphite Lithium-Ion Battery Cells. *Batteries & Supercaps* **2021**, *4* (8), 1344−1350.

(18) Yang, Y.; Zhou, J.; Rao, A. M.; Lu, B. Bio-inspired carbon electrodes for metal-ion batteries. *Nanoscale* **2024**, *16* (12), 5893−5902.

(19) Zheng, J.; Bock, D. C.; Tang, T.; Zhao, Q.; Yin, J.; Tallman, K. R.; Wheeler, G.; Liu, X.; Deng, Y.; Jin, S.; et al. Regulating electrodeposition morphology in high-capacity aluminium and zinc battery anodes using interfacial metal−substrate bonding. *Nature Energy* **2021**, *6* (4), 398−406.

(20) Wei, L.; Wang, S.; Men, S. Electronic Effects in the Structure of 1-Ethyl-3-Methylimidazolium Ionic Liquids. *Russian Journal of Physical Chemistry A* **2021**, *95* (4), 736−740.

(21) Corrales-Luna, M.; Le Manh, T.; Romero-Romo, M.; Palomar-Pardavé, M.; Arce-Estrada, E. M. 1-Ethyl 3-methylimidazolium thiocyanate ionic liquid as corrosion inhibitor of API 5L X52 steel in H_2SO_4 and HCl media. *Corros. Sci.* **2019**, *153*, 85−99.

(22) Aydogan Gokturk, P.; Salzner, U.; Nyulászi, L.; Ulgut, B.; Kocabas, C.; Suzer, S. XPS-evidence for in-situ electrochemically-generated carbene formation. *Electrochim. Acta* **2017**, *234*, 37−42.
(23) Beattie, D. A.; Arcifa, A.; Delcheva, I.; Le Cerf, B. A.; MacWilliams, S. V.; Rossi, A.; Krasowska, M. Adsorption of ionic liquids onto silver studied by XPS. *Colloids Surf., A* **2018**, *544*, 78−85.
(24) Lockett, V.; Sedev, R.; Harmer, S.; Ralston, J.; Horne, M.; Rodopoulos, T. Orientation and mutual location of ions at the surface of ionic liquids. *Phys. Chem. Chem. Phys.* **2010**, *12* (41), 13816−13827.
(25) *NIST X-ray Photoelectron Spectroscopy Database, NIST Standard Reference Database Number 20*, Version 5.0; National Institute of Standards and Technology, Gaithersburg MD, 2000. https://dx.doi.org/10.18434/T4T88K.
(26) Semiletov, A. M.; Chirkunov, A. A.; Grafov, O. Y.; Kuznetsov, Y. I. Stability of Supehydrophobic Layers Formed by Organic Acids on the Surface of Aluminum Alloy 6063. *Coatings* **2022**, *12* (10), 1468.
(27) Yoo, D.-J.; Heeney, M.; Glöcklhofer, F.; Choi, J. W. Tetradiketone macrocycle for divalent aluminium ion batteries. *Nat. Commun.* **2021**, *12* (1), 2386.
(28) Gursu, H.; Guner, Y.; Arvas, M. B.; Dermenci, K. B.; Savaci, U.; Gencten, M.; Turan, S.; Sahin, Y. Production of chlorine-containing functional group doped graphene powders using Yucel's method as anode materials for Li-ion batteries. *RSC Adv.* **2021**, *11* (63), 40059−40071.
(29) Petnikota, S.; Teo, K. W.; Chen, L.; Sim, A.; Marka, S. K.; Reddy, M. V.; Srikanth, V. V. S. S.; Adams, S.; Chowdari, B. V. R. Exfoliated Graphene Oxide/MoO_2 Composites as Anode Materials in Lithium-Ion Batteries: An Insight into Intercalation of Li and Conversion Mechanism of MoO_2. *ACS Appl. Mater. Interfaces* **2016**, *8* (17), 10884−10896.
(30) Lei, H.; Tu, J.; Yu, Z.; Jiao, S. Exfoliation Mechanism of Graphite Cathode in Ionic Liquids. *ACS Appl. Mater. Interfaces* **2017**, *9* (42), 36702−36707.
(31) Petnikota, S.; Rotte, N. K.; Reddy, M. V.; Srikanth, V. V. S. S.; Chowdari, B. V. R. MgO-Decorated Few-Layered Graphene as an Anode for Li-Ion Batteries. *ACS Appl. Mater. Interfaces* **2015**, *7* (4), 2301−2309.
(32) Petnikota, S.; Srikanth, V. V. S. S.; Toh, J. J.; Srinivasan, M.; Bobba, C. V. R.; Adams, S.; Reddy, M. V. Electrochemistry-related aspects of safety of graphene-based non-aqueous electrochemical supercapacitors: a case study with MgO-decorated few-layer graphene as an electrode material. *New J. Chem.* **2019**, *43* (25), 9793−9801.
(33) Petnikota, S.; Marka, S. K.; Banerjee, A.; Reddy, M.V.; Srikanth, V.V.S.S.; Chowdari, B.V.R. Graphenothermal reduction synthesis of 'exfoliated graphene oxide/iron (II) oxide' composite for anode application in lithium ion batteries. *J. Power Sources* **2015**, *293*, 253−263.

https://doi.org/10.1021/acsaem.4c00444
ACS Appl. Energy Mater. 2024, 7, 6862−6872